Age Induced Effects on ESD Characteristics of Solar Array Coupons After Combined Space Environmental Exposures

Kenneth H. Wright, Todd A. Schneider, Jason A. Vaughn, Bao Hoang, Victor V. Funderburk,

Frankie Wong, and George Gardiner

***Abstract*— A set of multi-junction GaAs/Ge solar array test coupons provided by Space Systems/Loral were subjected to a sequence of 5-year increments of combined space environment exposure tests. The test coupons capture an integrated design intended for use in a geosynchronous (GEO) space environment. A key component of this test campaign is performing electrostatic discharge (ESD) tests in the inverted gradient mode. The protocol of the ESD tests is based on the ISO standard for ESD testing on solar array panels [ISO-11221]. The test schematic in the ISO reference has been modified with Space System/Loral designed circuitry to better simulate the on-orbit operational conditions of its solar array design. Part of the modified circuitry is to simulate a solar array panel coverglass flashover discharge. All solar array coupons used in the test campaign consist of four cells constructed to form two strings. The ESD tests were performed at the beginning-of-life (BOL) and at each 5-year environment exposure point until end-of-life (EOL) at 15 years. The space environmental exposure sequence consisted of ultra-violet radiation, electron/proton particle radiation, thermal cycling, and Xenon ion thruster plume erosion. This paper describes the ESD test setup and the importance of the electrical test design in simulating the on-orbit operational conditions. Arc inception voltage results along with ESD test behavior from the BOL condition through the 15th year age condition are discussed. In addition, results from a Xenon plasma plume exposure test with an EOL coupon under the full ESD test condition will be discussed.**

***Index Terms*— Photovoltaic Cell Testing, Electrostatic Discharges, ESD, Space Environment Testing.**

Kenneth H. Wright is with the Center for Space Plasma and Aeronomic Research, University of Alabama-Huntsville, Huntsville, AL 35899 USA (e-mail: Ken.Wright@uah.edu)

Todd. A. Schneider, J. A. Vaughn are with the NASA/Marshall Space Flight Center, Huntsville, AL 35812 USA (e-mail: todd.a.schneider@nasa.gov; jason.a.vaughn@nasa.gov)

Bao Hoang, Victor V. Funderburk, Frankie K. Wong, George Gardiner, are with Space Systems/Loral., Palo Alto, California 940343 USA (email: Hoang.Bao@ssd.loral.com; funderbv@ssd.loral.com ; Wong.Frankie@ssd.loral.com; Gardiner.George@ssd.loral.com)

I. Introduction

AFTER nearly four years, a rigorous test campaign to determine the effects of the space environment on a solar array design is nearly complete. In 2008, Space Systems/Loral (SS/L) challenged NASA's Marshall Spaceflight Center (MSFC) to carry out a comprehensive test campaign which involved subjecting candidate solar cell coupons to all aspects of the geosynchronous (GEO) space environment while periodically gauging the electro-static and functional performance of the coupons.

Ultimately, the equivalent of 15 years of GEO space environment aging was applied to the solar array coupons in 5 year increments. All of the testing was carried out on the MSFC campus, which minimized the risk of sample damage as a result of packing and shipping. The environmental aging tests included ultra-violet radiation, high energy charged particle radiation, thermal cycling, and ion erosion. After each space environment was applied to a given coupon, a set of functional tests was conducted to determine the effect of the environment on the electrical performance of the coupon's cells and diodes.

To determine the effect of five years of equivalent space environment exposure on the electro-static charging properties of a given coupon, an Arc Inception Voltage test and an Electro-Static Discharge (ESD) test were performed. The results associated with the first 5-year ESD evaluation were described by Wright et al. in 2011 [1]. Interestingly, Wright et al. described a marked change in the arc inception voltage after the first 5-year equivalent GEO environment tests were complete. In this paper the Wright et al. results are compared to the results from the 10th year and 15th year tests.

At the completion of the GEO environment aging process, a worst-case scenario ESD test was performed in which the coupons with 15 years of equivalent aging were electrically charged and then subjected to a Xenon plasma plume from an electric propulsion thruster (commonly used on satellites for station-keeping). The goal of this test was to determine if the

"aged" coupon would experience an ESD event that would develop into a sustained or temporary sustained arc.

II. Test Plan

When Space Systems/Loral (SS/L) set out to evaluate the ability of their solar array design to withstand the harsh GEO environment for a typical 15-year lifetime, they realized there were advantages associated with dividing the testing into increments, as opposed to one continuous test. The advantages of dividing the test into three 5-year increments are: 1) Early insight into the direct effects of environment aging; 2) The capacity to adjust the process – if warranted; 3) The ability to spot trends in the effects of environmental aging.

The test plan developed by SS/L is characterized by two main processes which are repeated throughout the project. The first process is Evaluation - in which the performance of the coupon is measured. The second process is Environmental Exposure - where the coupon is subjected to a space environment for the equivalent of 5-years exposure.

TABLE I
COMPOSITION AND DESCRIPTION OF TESTS IN THE EVALUATION PROCESS

Test Name	Test Description	Performance Measured
LAPSS	Large Area Pulsed Solar Simulator testing illuminates the coupon with a simulated solar spectrum of light	Photovoltaic cell electrical output including: open circuit voltage (Voc), short circuit current (Isc) and maximum power (Pmax)
Dark I-V	The current (I) is measured as a function of voltage (V) with the photovoltaic cell(s) not illuminated by light (dark environment)	Response of photovoltaic cell current as a function of voltage. Output is a characteristic curve (I-V curve).
Bypass Diode	The electrical performance of a small diode built into the photovoltaic cell is measured by looking at the current flow as a function of voltage	Response of bypass diode as a function of applied current. Output is a characteristic curve (I-V curve).
AIV	Arc Inception Voltage testing measures the potential difference induced between the coverglass surface and the photovoltaic cell due to exposure to an electron beam	The voltage at which a primary arc is generated on the coupon
ESD	Electro-Static Discharge testing generates high current arcs on the coupon by allowing the arcs to source a capacitance which is equivalent to a full size solar array.	The division of current through the photovoltaic cells on a coupon. The susceptibility of the coupon to form secondary arcs.

The Evaluation process, which initiates the test program, starts with the coupon at Beginning-of-Life (BOL). The BOL evaluation establishes a baseline for evaluating performance. The Evaluation process is made up of multiple tests to fully characterize the coupon. Table I provides a breakout and description of the tests that comprise the Evaluation process.

TABLE II
COMPOSITION AND DESCRIPTION OF TESTS IN THE ENVIRONMENTAL EXPOSURE PROCESS

Environment	Range	Flux or Duration	Five Year Equivalent Amount
High Energy Electrons	1 MeV	1×10^{-9} A/cm^2	2.7×10^{14} electrons/cm^2
High Energy Protons	40 keV	5×10^{-9} A/cm^2	2.6×10^{15} protons/cm^2
Ultra-violet Radiation	230 to 400 nm	2-3 Suns	667 Equivalent Sun Hours
Ion Erosion	250 eV Xenon ions	115 micro-A/cm^2	1.21×10^{19} ions/cm^2
Thermal Cycle	-180 C to +95 C	2 C per min.	440 cycles
Full Power ESD Arc	7 - 28 Amps	150 micro-seconds	10 arcs

The Environmental Exposure process, like the Evaluation process, is made up of multiple individual tests that effectively "age" the coupon by subjecting it to an accelerated exposure of a particular element within the GEO environment. Due to the wide range and disparate nature of the elements that make up the GEO environment, it is not possible to apply all of the environments using a single test system. However, MSFC does have the unique capability to perform all of the environmental exposures inside a very small radius (200 meters) within the MSFC campus. In Table II the details associated with the Environmental Exposure process are provided. It should be noted that ESD testing is included in the Environmental Exposure process as well as the Evaluation process. This is due to the fact that the magnitude of the ESD arc currents is high enough such that the arcs can change the performance of the photovoltaic cells in a manner comparable to some of the other GEO environments.

In Figure 1 the test plan structure and sequence is shown. From this figure it can be seen that the Evaluation process is interleaved throughout the test campaign in order to gauge the effects of a given environment on the coupon. The test plan culminates in a step called "SPT Interaction" testing. In this step, a coupon in an ESD test configuration is charged by an electron beam and then impacted by an electric propulsion thruster plume. The thrusters used by SS/L are referred to by the model name "SPT", hence the name "SPT Interaction Test". The purpose of the SPT Interaction test is to determine if a secondary arc (sustained arc) will form on the coupon when it is

in its worst-case End-of-Life (EOL) condition.

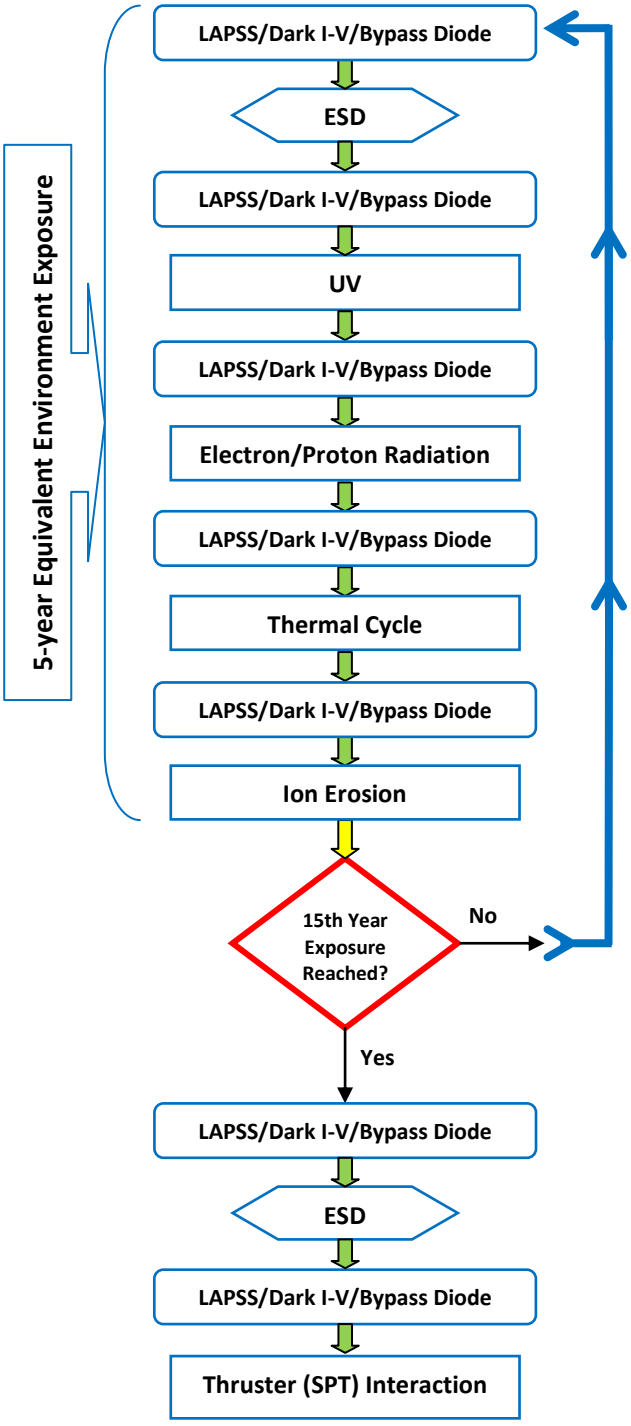

Fig. 1. Test plan flow diagram.

To help minimize the influence of small manufacturing differences, SS/L planned for three (3) samples to undergo the full 15 year test cycle as illustrated in the test plan shown in Fig. 1. The coupons were labeled "A", "B", and "C". One additional coupon, labeled "D", was included in the sample pool as a reserve. The reserve coupon could be used in the event an anomalous failure was encountered, or if a human error, for example during installation into a test system, caused physical damage to a coupon.

All of the test samples shared a common design and were constructed in the same manner by a single manufacturer. Fig. 2 is a picture of one of the samples. Each sample is composed of four (4) individual photovoltaic cells each with an integrated bypass diode. Two independent "strings" of cells are formed by connecting two cells together in series to form a single string. As shown in Fig. 2, the string on the left side of the coupon is string 1 and string 2 is on the right side of the coupon. Both strings are mounted on a Kapton sheet which is applied to a substrate structure composed of an Aluminum honey-comb core with graphite face sheets. The substrate is constructed with holes in all four corners which provide a pass-through for the string wires and can be used for sample mounting. An insulating bushing is inserted in each corner hole to help isolate the pass-through wires from the grounded honey-comb structure. The size of the coupon and the limitation to a 2x2 cell format is dictated by the test volume in the radiation target chamber.

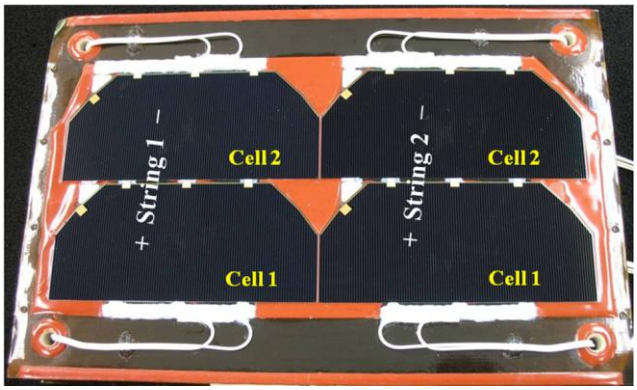

Fig. 2. Picture of typical test coupon. The coupon has been configured in to two strings with each string composed of two cells.

The current test status of each sample is shown in Table III. As can be seen, the test program is nearly complete. With the exception of coupon C, all of the samples followed common trends with respect to performance changes, and overall, showed excellent functionality under the worst-case conditions. Coupon C was removed from test due to a failure in a semiconductor layer/junction in a small region of string-1/cell-2. Given that all of the other elements on coupon C were unaffected, and that the 8 cells associated with the other two coupons were not affected, the failure of string-1/cell-2 was deemed anomalous. In all likelihood, the problem with the one cell on coupon C can be attributed to a defect in the semiconductor material developed during the manufacturing process. Variability in the efficiency of photovoltaic cells due to semiconductor manufacturing issues has been well characterized [2]-[4]. It is not surprising then that a single cell – manufactured in a large batch process – might contain a small defect which diminishes its performance.

The insertion of the reserve coupon (coupon D) into the test flow occurred after coupons A and B had completed their 5th

year evaluation. Therefore, coupon D was out of phase with the other coupons' test schedule. However, final tests on coupon D are underway, and it is anticipated that the overall test campaign will draw to a close by the end of May 2012.

TABLE III
TEST COMPLETION STATUS FOR ALL SAMPLE COUPONS

	Status			
Test Phase	**A**	**B**	**C**	**D**
5th-year Environment	Complete	Complete	Complete	Complete
5th-year Evaluation	Complete	Complete	Complete	Complete
10th-year Environment	Complete	Complete	Stopped Testing*	Complete
10th-year Evaluation	Complete	Complete	N/A	Complete
15th-year Environment	Complete	Complete	N/A	In progress
15th-year Evaluation	Complete	Complete	N/A	May 2012
SPT Interaction Test	Complete	Complete	N/A	May 2012

* Removed from test due to an anomalous failure of cell 2 in string 1.

III. ESD TEST SETUP

Recognizing the impact that a long duration electrical arc can have on the performance of a spacecraft power system [5], the SS/L team emphasized ESD testing in their overall strategy by employing three different ESD test scenarios: 1) Arc Inception Voltage, 2) Full Power ESD Arc, and 3)Thruster Plume Interaction (referred to as "SPT Interaction" by SS/L). While the ESD tests are based on the prescription set forth in the ISO-11221 Test Standard [6], each test setup has some important features that are worth noting. In this section, a brief description of the key features of each ESD test setup employed by MSFC is provided along with a circuit diagram. Additional information about the AIV and Full Power ESD Arc tests has been previously provided by Wright et al. and Hoang et al. [1], [7].

A. Arc Inception Voltage Test Setup

The purpose of the AIV test is to determine the potential difference that must exist between the substrate and elements on the front surface of the coupon in order for an arc to be generated. This test is not concerned with arc current magnitudes and no provision for secondary or sustained arcs is included in the circuit arrangement. Therefore, all of the photovoltaic cells and the substrate can be tied together electrically. Also, the arc energy is intentionally kept low, so that arc damage is very unlikely. This provides the test conductor with the freedom to generate multiple arcs without worrying about damaging the coupon – thereby increasing the statistical sample for the AIV measurement.

The AIV test circuit is shown in Fig. 3. In the diagram the label "CP" indicates a current probe. The arrow over the CP label indicates the direction of positive current flow needed to produce a positive polarity output signal. The component labeled "V" is a high voltage probe.

To carry out AIV testing, the coupon cells and substrate are biased to -5 kV. Then an electron beam is directed at the coupon such that it impinges on the front side of the coupon where the photovoltaic cells and coverglass are located. With a judicious choice of electron beam energy, one can excite secondary electrons from the coverglass such that the potential of the coverglass is made more positive than the photovoltaic cells and substrate. The potential of the coverglass is periodically measured with a non-contact probe. Eventually, a potential difference of sufficient magnitude to form an arc is created between the coverglass and another element (e.g. photovoltaic cell, interconnect, bus bar, etc.) on the front surface. The potential difference that results in an arc is referred to as the Arc Inception Voltage (AIV).

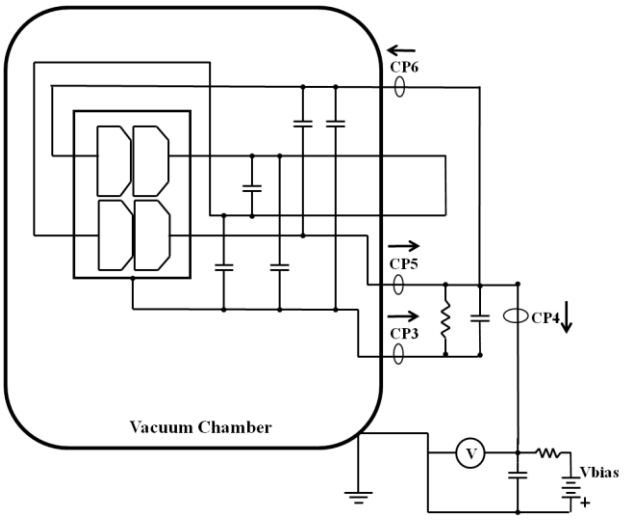

Fig. 3. Arc Inception Voltage (AIV) test circuit. "CP" indicates the location of a current probe and "V" indicates the location of the high-voltage probe.

In the interest of repeatability and accuracy, the following procedure was employed for the determination of the AIV:

1. Apply -5 kV bias to substrate using Vbias supply.
2. With a Trek probe, verify that the coverglass surface is at -5 kV.
3. Set electron beam to 5.9 keV. With the coverglass surface at -5kV and the electron beam energy at 5.9 keV, the electrons impacting the coverglass surface will have net energies of 900 eV. This value is near the peak in the secondary emission curve. See for example Kawakita et al. [8].
4. Expose coupon to electron beam flux of 1-2 nA/cm^2 for a

limited time.

5. Measure coverglass potential with Trek probe.
6. Based on the value of the coupon surface potential, select electron beam energy to be 900 V greater in magnitude. For example, if the measured coverglass surface potential is -4.5 kV, the electron beam energy selected would be 5.4 keV. By always having the electrons impact the coverglass surface with ~ 900 eV, some consistency can be established in the expected change in coverglass potential between electron exposures.
7. Repeat steps 5 and 6 until an arc occurs.

Changes in the coverglass potential are a function of the electron beam energy and the total number of electrons applied (fluence). The MSFC team used a computer controlled electron source which allowed for precise control of the electron beam exposure times. Typically, the electron beam flux was held constant and the amount of exposure time was varied. This helped make the coverglass potential changes a more controlled process.

B. Full Power ESD Arc Test Setup

In stark contrast to the AIV Test, the Full Power ESD Arc Test is focused on generating high current arcs that have the potential to initiate secondary arcs – such as sustained arcs. The Full Power ESD Arc test not only creates high current arcs by increasing the size of the primary arc pulse capacitor, but as can be seen in Fig. 4, several additional circuit elements are added to increase the fidelity of the test circuit such that it is as close to the actual spacecraft power system as possible. One key element in the circuit is the Solar Array Simulator (SAS) power supply which provides a voltage between the two strings. The presence of a voltage difference between strings opens the door to secondary arc generation, which can generate significant damage.

Prior to performing a Full Power ESD Arc test, the circuit in Fig. 4 is balanced such that the voltage drop across a string and between strings precisely compares to the actual spacecraft power system operating points. With balancing complete, a -5 kV bias is applied to the cells via the principal charging capacitor. Using the information learned in the AIV test, an electron beam is applied to the side of the coupon with the photovoltaic cells and coverglass. A so-called "inverted gradient" condition [6] is achieved between the coverglass and the cells (or bus bar components). When the AIV condition is met, a high-current long duration ESD primary arc is formed.

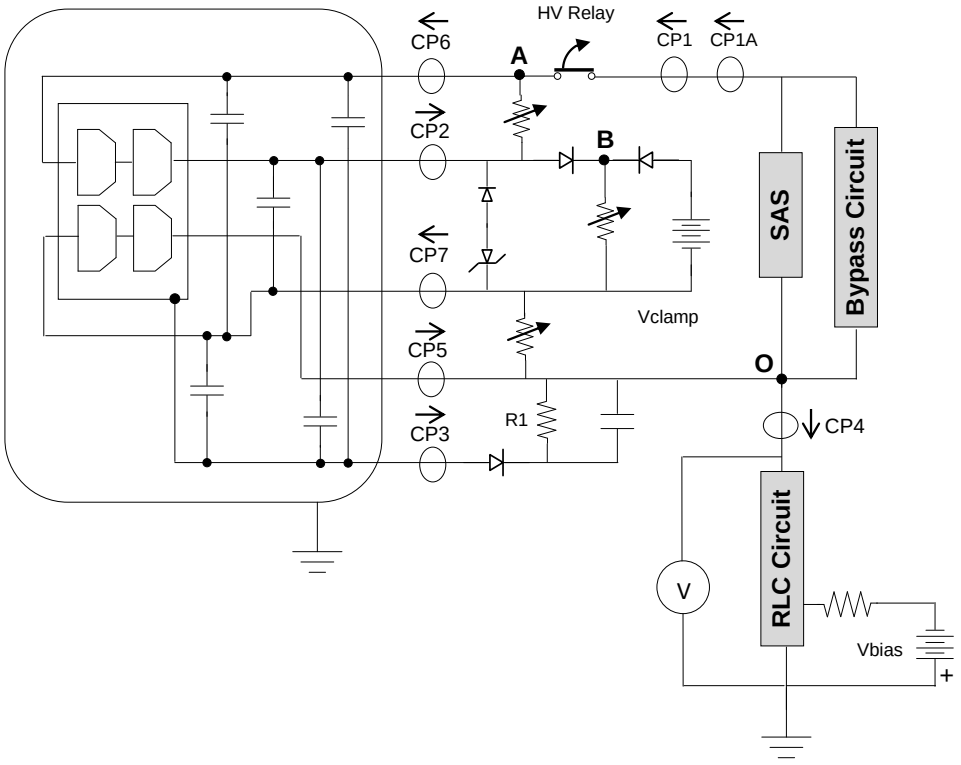

Fig. 4. ESD test circuit. "CP" indicates the location of a current probe and "V" indicates the location of the high-voltage probe. "A" and "B" indicate voltage measurement locations referenced to the point "O".

C. Thruster Plume Interaction (SPT Interaction)
Test Setup

The SPT Interaction Test is really an extension of the Full Power ESD Arc test. The same circuit and coupon bias conditions created in the Full Power ESD Arc Test are implemented for the SPT Interaction Test; however, the electron beam application is stopped before an ESD arc can occur. With the sample in an inverted gradient condition and poised to arc, the plume from an electric propulsion thruster is directed at the sample.

The electric propulsion thrusters used on SS/L satellites are typically Hall-Effect thrusters known by their model name as "SPT" thrusters [9]. The SPT devices produce thrust by creating and accelerating Xenon ions. To avoid space charge problems associated with the production of all positively charged ions, a low energy electron population is introduced near the thruster exit plane. The result is a high-density plasma with 250 eV drifting Xenon ions and low temperature electrons [10].

Multiple SPT thrusters are employed on SS/L spacecraft and all sections of solar arrays are subject to being impinged by the thruster plume. The density and temperature of the plasma contacting the solar array depends on the relative location of the array section with respect to the thruster output plane. A solar array section far away from the thruster will see a greatly reduced flux of ions compared to a section that is very close to the thruster. Using thruster plume modeling software, SS/L determined the flux range expected for a typical satellite, and from this range, chose a low, medium, and high flux value to be used in the SPT Interaction test. Table IV shows the target flux levels established by SS/L
.

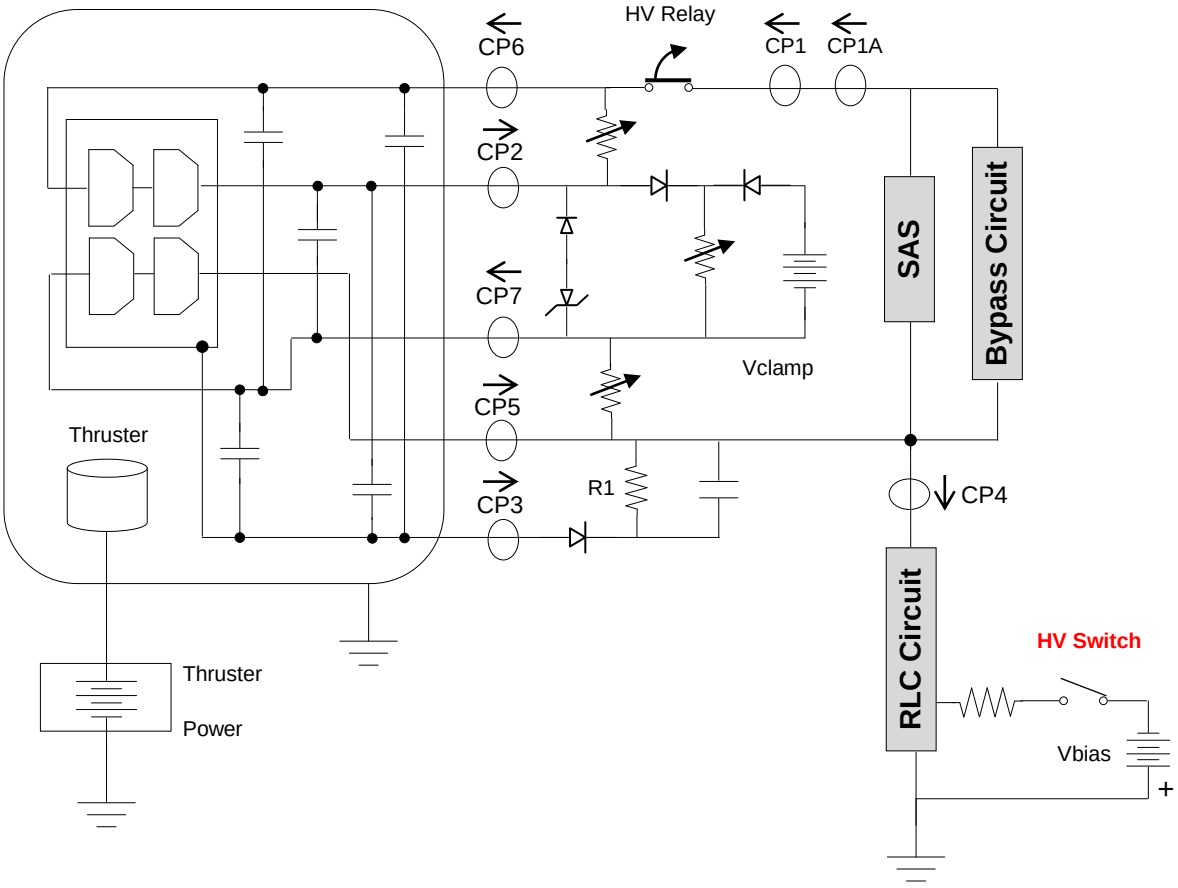

Fig. 5. Thruster Plume (or SPT Interaction) test circuit. "CP" indicates the location of a current probe. A High Voltage switch is added to the charging circuit to stop the re-charging of the system during a thruster firing.

TABLE IV
FLUX LEVELS SPECIFIED BY SS/L FOR THE XENON ION BEAMS USED DURING SPT INTERACTION TESTS

Target Flux	Acceptable Flux Range	Xenon Ion Energy
1 nano-A/cm^2	1-5 nA/cm^2	250 eV (+/- 10 eV)
100 nano-A/cm^2	100 – 125 nA/cm^2	250 eV (+/- 10 eV)
10 micro-A/cm^2	> 4 micro-A/cm^2	250 eV (+/- 10 eV)

To achieve the wide range of the flux levels specified by SS/L, the MSFC team chose to employ a gridded Kaufman type [11],[12] electric propulsion thruster instead of an actual SPT device (Hall Effect thruster). The Kaufman thruster allows the flux to be easily adjusted by changing current and voltage settings in the thruster power system. However, a SPT thruster has a very limited range of power settings that can be employed and still maintain a steady ion beam output. The only option to change the flux levels seen by a sample in a SPT plume is to physically change the distance between the sample and the thruster exit plane. MSFC vacuum chamber space limitations (and vacuum pumping limitations) did not allow for the option of using an actual flight SPT thruster in the test. Instead a very close representation of the SPT thruster plume was created by the MSFC team using their Kaufman thruster.

Fig. 5 contains a schematic of the SPT Interaction test circuit. When compared to the Full Power ESD Arc test circuit (Fig. 4) one can see there is a small modification to the principal capacitor charging circuit. A switch was added to that circuit whose purpose is to prevent the capacitor from charging when the switch is opened. The switch was added to limit the discharge of the coupon to one event per thruster plume application. Procedurally, the switch is opened after the inverted gradient condition is established on the coupon, but just prior to the generation of a thruster plume (ion beam). By doing this, the high voltage capacitor (and cells) would not be able to recharge during the ion beam interaction period – which was typically 120 seconds in duration. Limiting the high voltage charging (or recharging) during the thruster firing is consistent with actual on-orbit operations.

IV. ESD TEST RESULTS

Presently, the ability to accurately predict the location, magnitude, and impact of ESD arcs on solar arrays is limited. New analytical models can generally predict the surface charging that might occur on an array, but accounting for small deviations in edge geometries or gap spacing over a large area is not practical. To further complicate matters, the space environment tends to degrade materials over time, which can result in cracks in insulating materials and the formation of new arc sites. Consequently, the only practical means for determining the ESD performance of solar arrays is testing.

To fully characterize the performance of their solar array design under electrostatic charging and discharging conditions, the SS/L team called for two separate ESD tests to be conducted at each stage of environmental aging, which were: Beginning-of-Life (BOL), 5-year equivalent, 10-year equivalent, and 15-year equivalent. A third ESD test was executed after the 15-year equivalent stage to determine how an array with maximum material degradation would react to worst-case charging conditions. A summary of test results for each sample coupon are provided below and are organized by the type of ESD test and the stage of environmental exposure (on-orbit equivalent aging).

A. Arc Inception Voltage (AIV) Test Results

Given that the AIV test is performed with low arc energies, and therefore low risk for material damage, it was common to generate as many as 8 arcs on a coupon for a single AIV test. In Table V the mean value of each AIV test (on a given coupon) is presented as a function of equivalent age. Interestingly, a marked change in AIV occurred for each coupon after the 5th year environmental aging was complete. After the 5th year change, however, the AIV remained relatively constant.

TABLE V
AVERAGE ARC INCEPTION VOLTAGE (AIV) FOR ALL COUPONS AT EACH STAGE OF ENVIRONMENTAL AGING

Average Arc Inception Voltage				
Coupon	BOL	5th Year	10th Year	15th Year
A	2860	560	630	630
B	3060	410	600	640
C	2750	660	N/A	N/A
D	2980	840	1150	TBD

Due to the fact that all of the space environments (UV, Radiation, Thermal Cycle, and Ion Erosion) were applied to each coupon between the BOL and 5th year equivalent stage, it is not possible to determine if a single environment is responsible for the change in AIV, or if it is indeed the combination of environments.

To understand the factors that have contributed to the lowering of the AIV, the authors have considered the fundamental aspects of arc generation (Wright et al.). The formation of an arc occurs when an electric field threshold is reached – typically at an interface point. The electric field,

however, is a function of potential and distance. Given that the applied potentials on the surface of the coupons during AIV testing were the same between the BOL and 5th year test; it suggests that a change in distance at the arc locations may have been responsible for the shift in AIV. The authors suggest that changes in the RTV grout (used to insulate sections of the array coupon) occurred as a result of hardening due to UV and charged particle radiation combined with mechanical stresses from thermal cycling. The creation of small gaps at a cell edge due to RTV insulation movement like that shown in Fig. 6, for example, could create a scenario where a moderate potential is created over a small distance, which results in a strong electric field – sufficient to create an arc.

Inspection of the test samples after the 5th year aging did reveal some changes to the RTV materials which would support the author's hypothesis on the factors that might contribute to the AIV change; however, without conducting a controlled investigation on this specific scenario, it is not possible to determine if it is indeed the root cause of the change. While such an investigation was outside of the scope of the project, it nevertheless remains as a task that could deliver important data to the aerospace community.

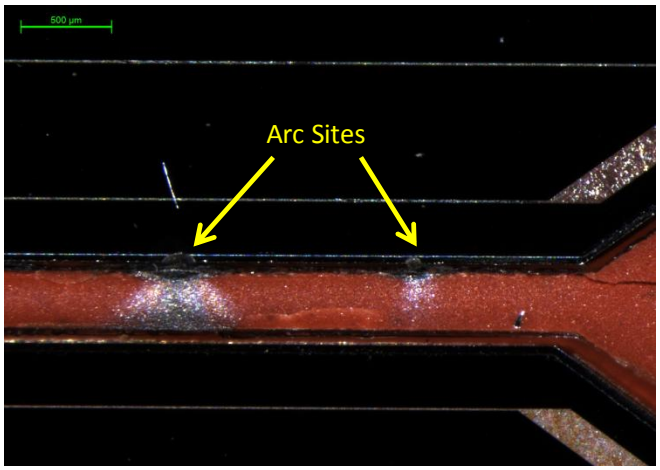

Fig. 6. Magnified image of a section of the area between strings on coupon A. The image reveals that the RTV contact with the cell edges is reduced and gaps have been created that allow for arc formation.

B. Full Power ESD Arc Test Results

Prior to initiating the test campaign at MSFC, the SS/L team analyzed their solar array design and determined the characteristics (magnitude and duration) of a primary arc pulse which represented a worst-case arc in the center of a solar array panel which sourced all of the charge in the panel capacitance [6],[13]. The total charge in the array capacitance was determined from the equation:

$$Q = C/V \qquad (1)$$

where Q is total charge, C is capacitance, and V is voltage. The voltage used by SS/L was based on earlier Arc Inception Voltage tests at Kyushu Institute of Technology (KIT) of new solar array sample coupons at BOL. The results of the SS/L analysis was a primary arc pulse based on 2,000 volts AIV with a peak current of 28 amps. Fig. 7 is an example of the primary arc pulse waveform.

To generate the primary arc pulse, SS/L designed an RLC-based pulse forming circuit which produced the desired peak current and limited the duration of the pulse to approximately 150 micro-seconds. The primary arc pulse circuitry is shown in the lower right portion of the circuit diagram in Fig 4 and Fig. 5. The MSFC test setup used a 28 Amp pulse-forming circuit even though AIV testing showed that the values obtained were greater than 2000V. This was done in part to preserve the test circuit configuration between MSFC and KIT.

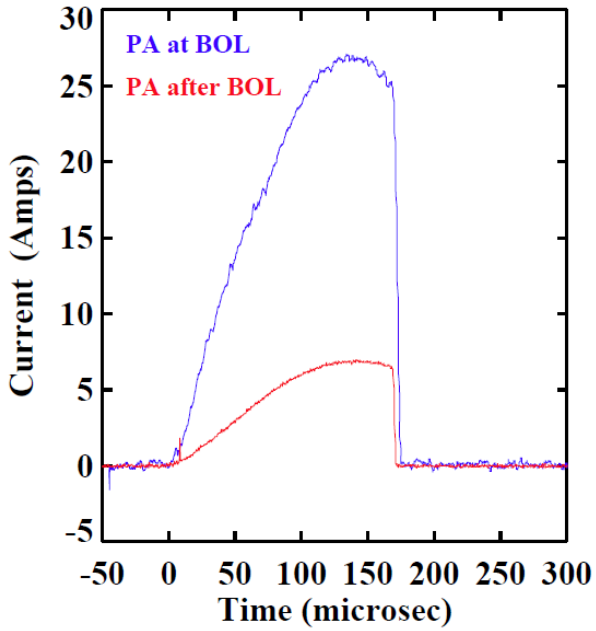

Fig. 7. Primary Arc (PA) measured waveform. The BOL waveform had a peak current of 28 Amps. The 5-year (and later) waveform has a peak current of 7 Amps. The change was implemented in the RLC circuitry after the Arc Inception Voltage decreased significantly after the 5-year equivalent exposure was complete.

When the AIV data from the post 5-year evaluation revealed a significant change in the inception voltage, the SS/L team reassessed their primary arc pulse calculations. The reduction in the mean arc inception voltage meant that the total charge contained in the primary pulse should be proportionally lower. SS/L arrived at a primary arc pulse with a peak current of 7 amps. An example of the lower magnitude primary arc pulse is shown in Fig. 7. The 7 amp peak current was chosen as a value that would reflect the new AIV conditions and yet still preserve some of the worst-case test margin that was part of their original test plan.

The Full Power ESD Arc test is intended to bring together the primary arc pulse with powered strings of photovoltaic cells. To achieve this configuration, the primary arc pulse circuit is tied to a Solar Array Simulator (SAS) power supply circuit. The SAS power supply is connected to the coupon such that a voltage is developed between the two strings. In the MSFC test, two separate string voltage conditions were investigated: 54 volts and 108 volts. The SAS power supply current output was limited to 0.55 amps for both inter-string voltage conditions. The presence of the inter-string voltage brings into play the possibility of developing a secondary arc between strings [14]. A secondary arc is formed when the plasma from a primary arc creates a low impedance path between cells in two different strings. Power from the strings can then be conducted through the secondary arc resulting in a so-called sustained arc, which, as the name suggests, is a long duration arc which can potentially damage array components including the photovoltaic cells [15].

Figs. 8-11 show a typical set of voltage and current data for a Full Power ESD Arc test. The data was obtained from coupon A after the 10th year equivalent environment exposure stage. The currents shown in the plots are measured by the Current Probes (CP) designated in Fig. 4. Similarly the voltages shown correspond to the measurement points called out in Fig. 4. For example "VAO" refers to the voltage measured between points "A" and "O".

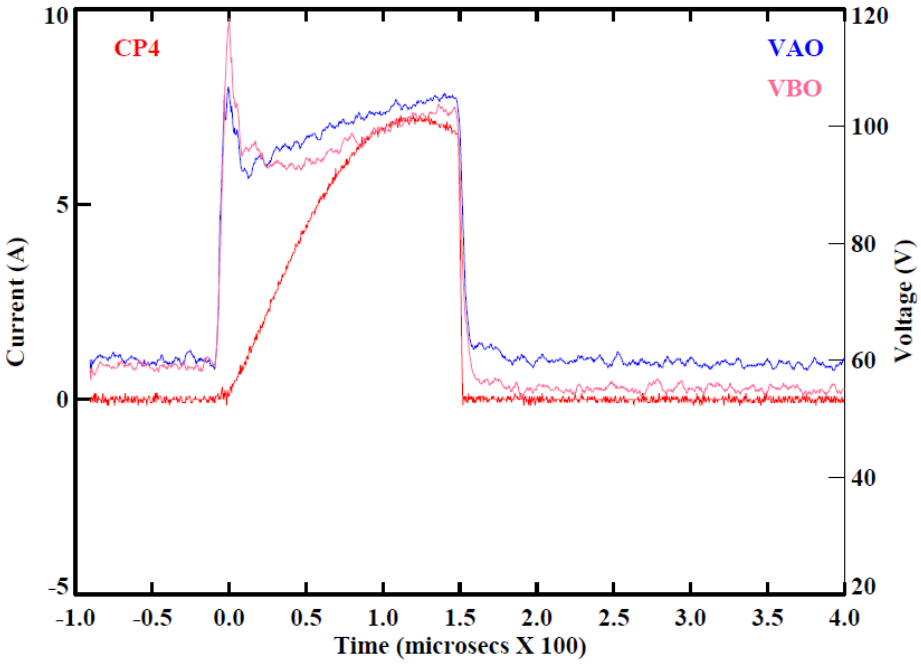

Fig. 8. Full Power ESD arc waveforms obtained from testing coupon A at its 10th year environmental age point

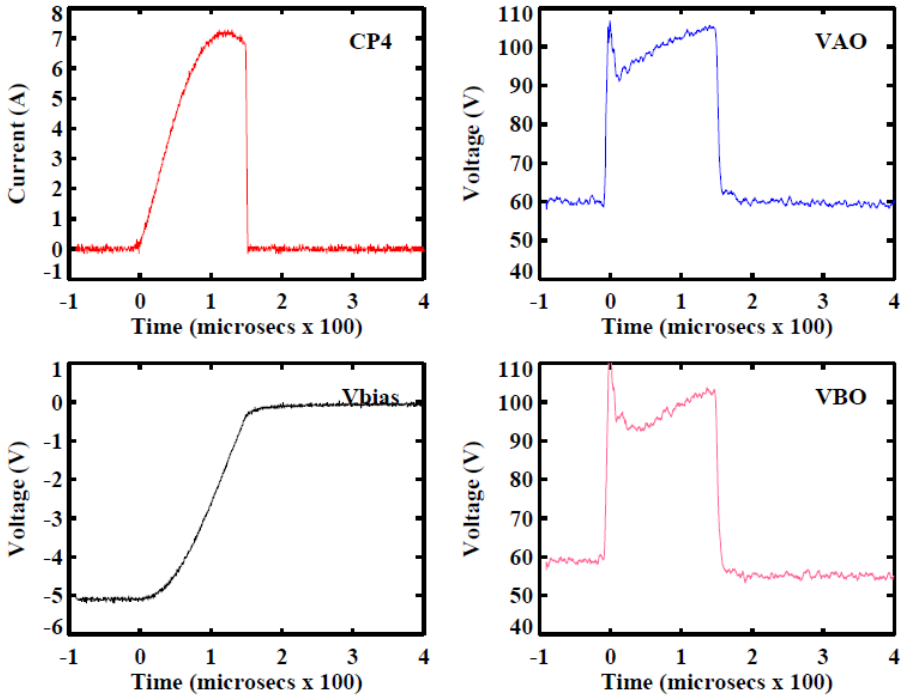

Fig 9. Full Power ESD arc waveforms obtained from testing coupon A at its 10th year environmental age point.

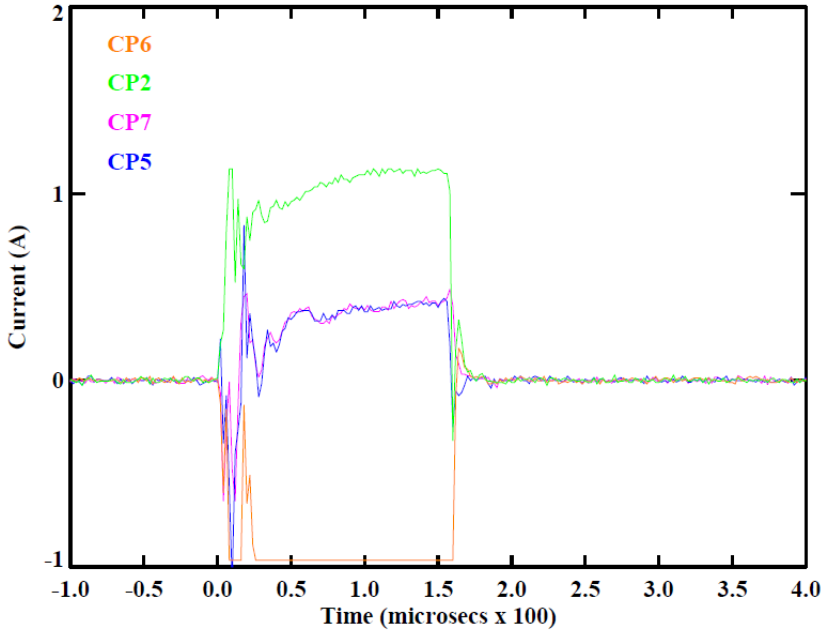

Fig.10. Full Power ESD arc waveforms obtained from testing coupon A at its 10th year environmental age point

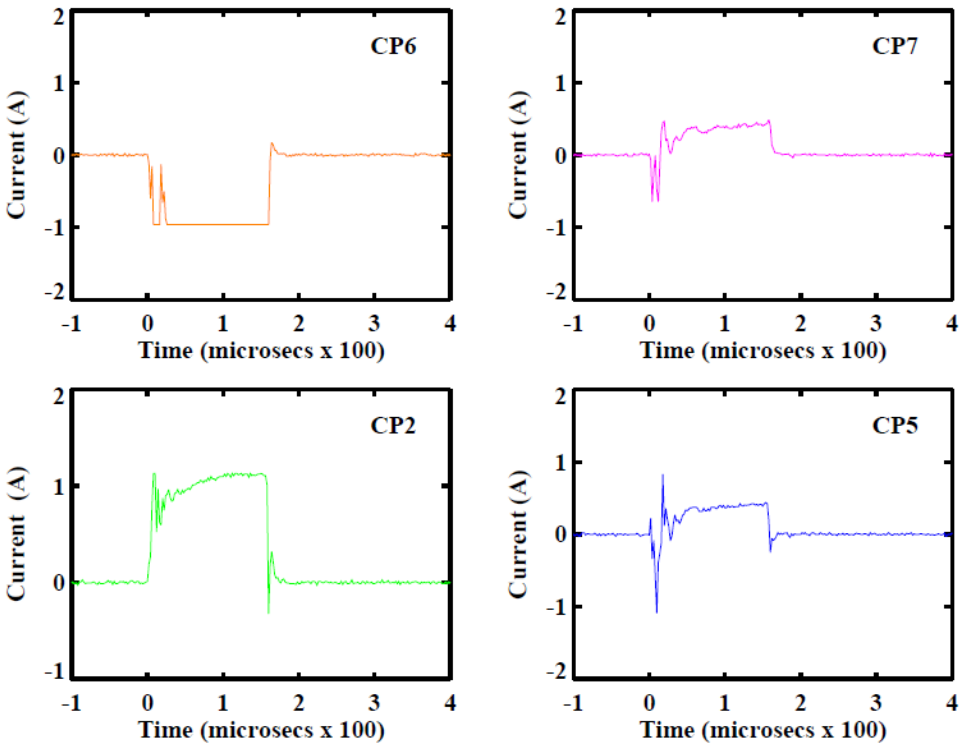

Fig. 11. Full Power ESD arc waveforms obtained from testing coupon A at its 10th year environmental age point.

In Fig. 12 the bright spot in the image is the visible flash corresponding to the ESD arc. The location of this bright spot is on string 1. The arc current path through the ESD circuit (Fig. 4) can be determined by looking at the CP waveforms. The majority of the current goes through CP6 and CP2 which confirms that the arc occurred on string 1.

Fig. 12. Image of arc flash on Coupon A string 1.

Establishing trends and looking for patterns was one of the goals of the test program setup by SS/L. Identifying a pattern in the location of the ESD arcs was one of the top analysis priorities. If, for example, there was found to be a concentration of arcs on a point common to each sample, then it would be possible to change the design of that point to limit the arcing on future solar array panels. Figs. 13-15 provide a set of "maps" of the arc site locations as a function of environmental age.

From the arc site maps in the Figs. 13-15 the following observations can be made:

- Coupons A and B tended to have the majority of arcs occur on the string 2 side of the coupon, whereas coupon D revealed the opposite behavior
- Interconnects and Bus Bars were common arc sites on all of the coupons
- In several cases, multiple arcs (>5) occurred in the same location
- The area between strings (i.e. between adjacent cells in separate strings) was not a common location for arcs

As the coupons aged, preferred arcs sites became the cell edges and corners. Due to the low occurrence of arcs between strings, the likelihood of a temporary sustained or sustained arc is diminished.

The total number of Full Power ESD Arcs for each coupon was at least 80. Out of this cumulative large number of induced arcs for all coupons, only one temporary sustained arc was documented. This result suggests that the SS/L array design is quite robust. Fig. 16 shows the arc locations for the single temporary sustained arc which occurred on coupon A after the equivalent of 15 years of aging. Figs. 17-20 shows the current and voltage waveforms associated with this event. A temporary sustained arc is characterized by an extension of the arc current beyond the cutoff of the primary arc pulse. The CP4 data provides the primary arc pulse current, and, by design, that pulse is about 150 microseconds in duration with a sharp cutoff as the current goes to zero. When CP6, CP2, CP7, and CP5 data is compared with CP4, one can see the extension of the 0.55A current ~ 60 microseconds beyond the primary arc pulse.

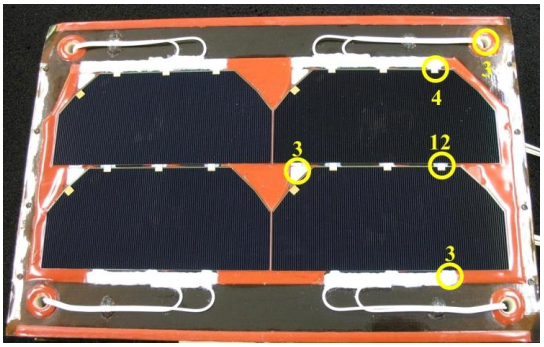

Coupon A - BOL

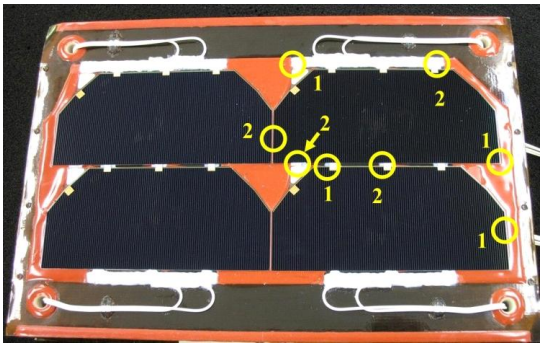

Coupon A – 5th Year

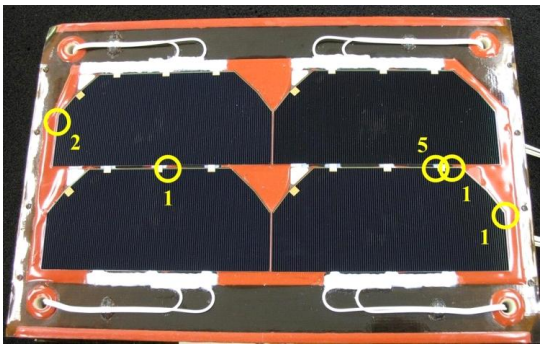

Coupon A – 10th Year

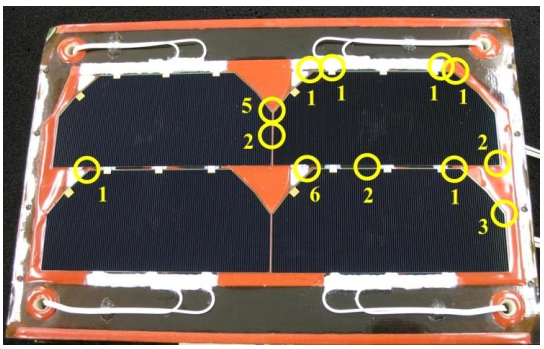

Coupon A – 15th Year

Fig.13. Full Power ESD Arc site locations on Coupon A. The number beside each circle indicates the number of times an arc occurred at that location

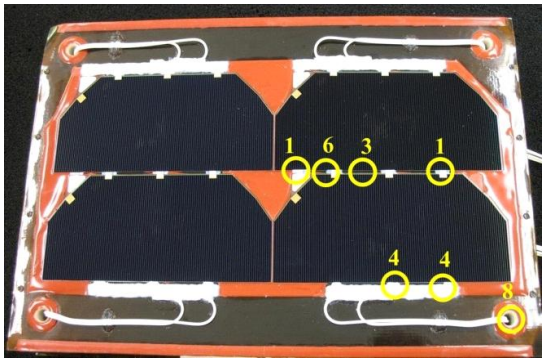

Coupon B - BOL

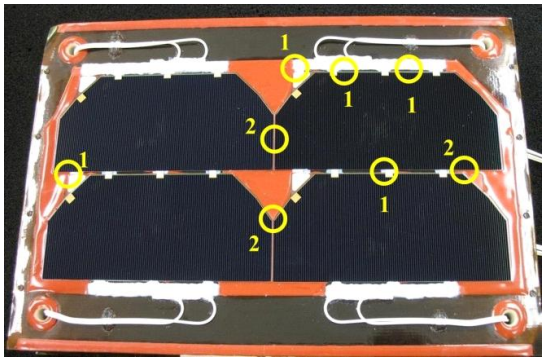

Coupon B – 5th Year

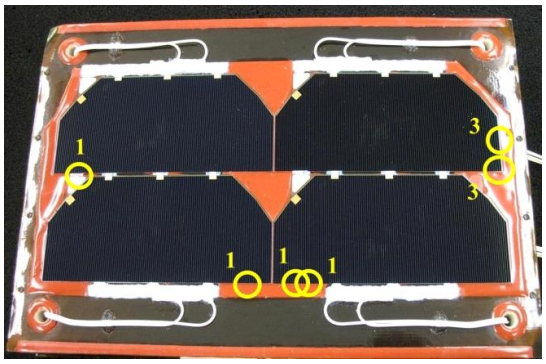

Coupon B – 10th Year

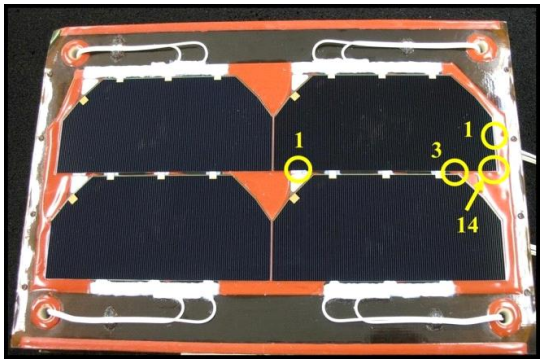

Coupon B – 15th Year

Fig. 14. Full Power ESD Arc site locations on Coupon B. The number beside each circle indicates the number of times an arc occurred at that location.

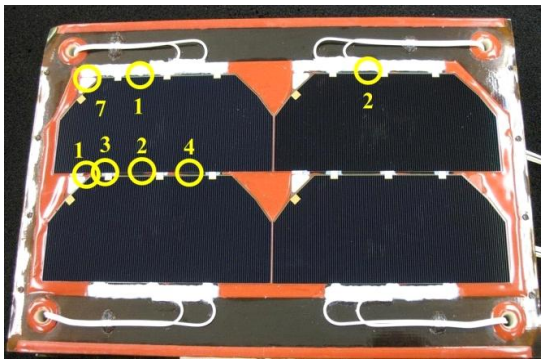

Coupon D - BOL

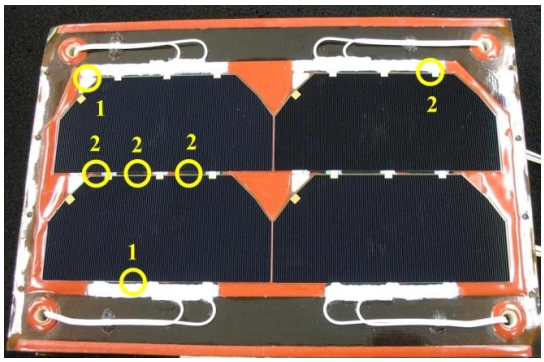

Coupon D – 5th Year

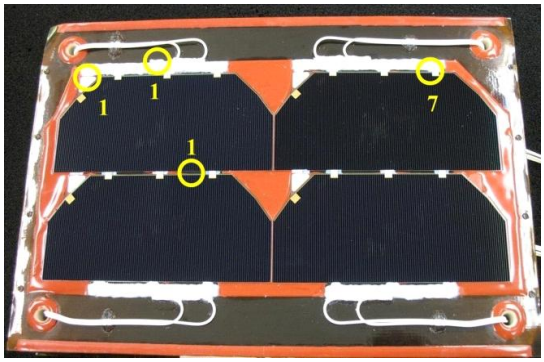

Coupon D – 10th Year

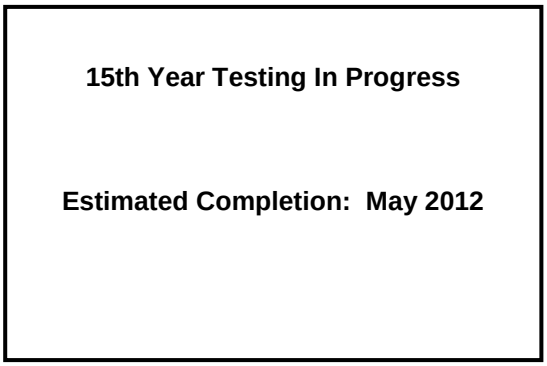

Coupon D – 15th Year

Fig. 15. Full Power ESD Arc site locations on Coupon D. The number beside each circle indicates the number of times an arc occurred at that location.

The image of the coupon in Fig. 16 reveals that two flashes occurred during the temporary sustained arc event. As expected, one flash occurred on string 1 and the other on string 2. This is evidence that a plasma bridge was formed between the two arc sites. SAS power supply current (limited to 0.55 amps) was then allowed to flow between the strings, as evidenced in CP6, CP2, CP7, and CP5. The very short duration of the flow of current between strings combined with the rarity of the event, suggests that the SS/L operational design is sound, and very unlikely to yield a damaging sustained arc.

Fig. 16. Arc site locations for the temporary sustained event on coupon A during the ESD test at its 15th year age point.

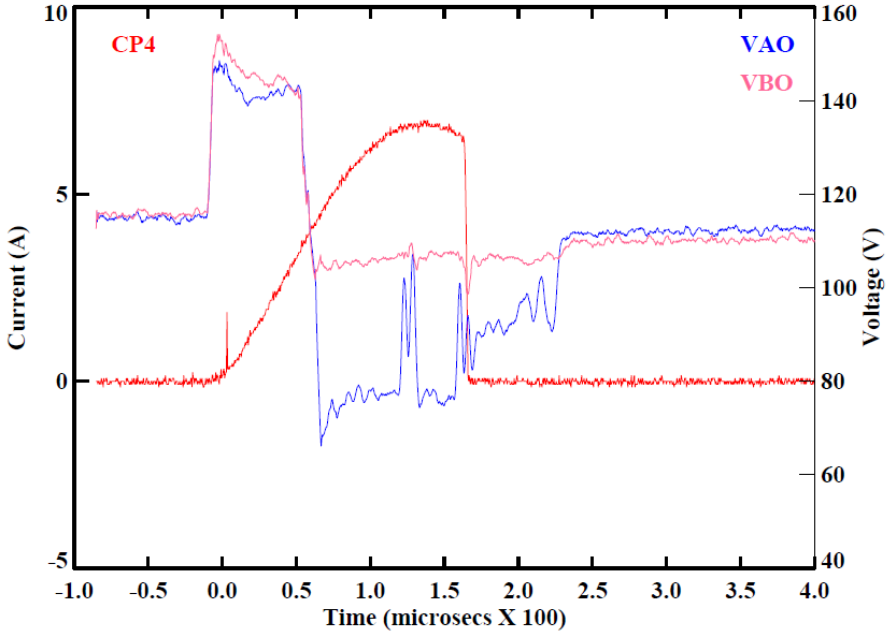

Fig. 17. Measured current and voltage for a Full Power ESD Arc for the temporary sustained event on coupon A during the ESD test at its 15th year age point..

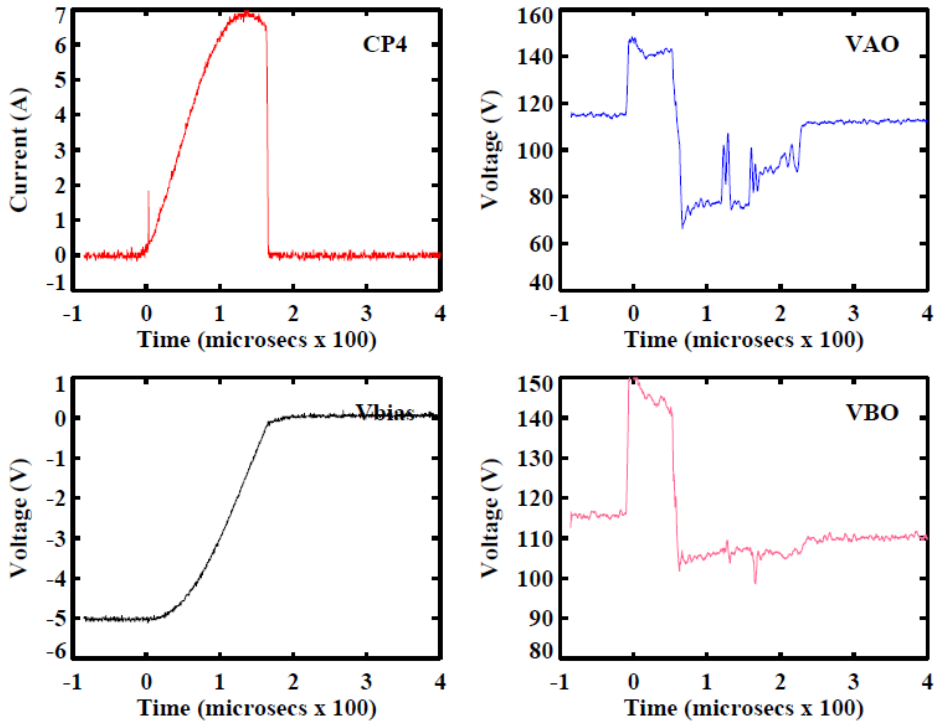

Fig. 18. Measured current and voltage for a Full Power ESD Arc for the temporary sustained event on coupon A during the ESD test at its 15th year age point.

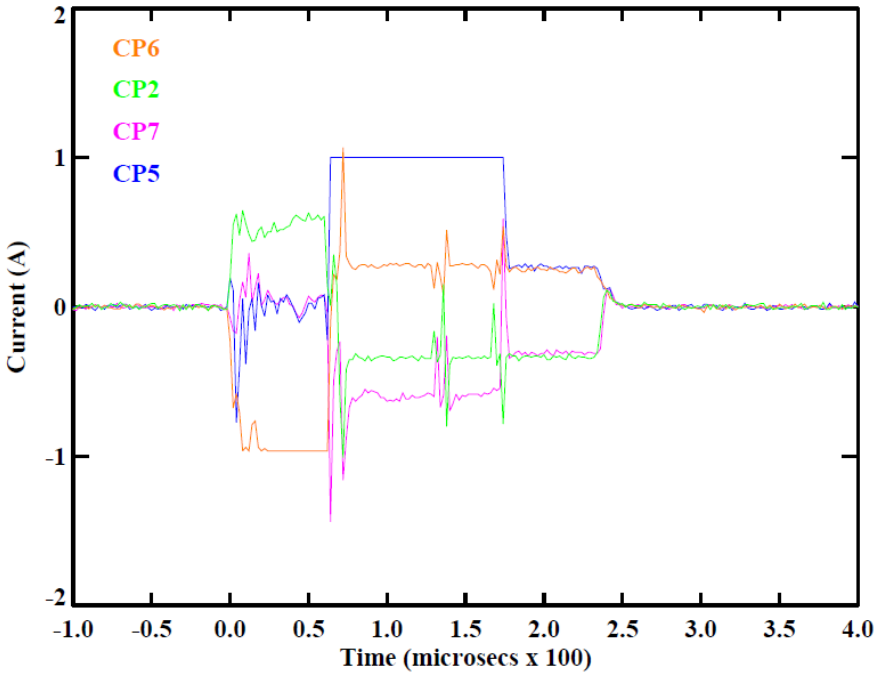

Fig. 19. Measured current for a Full Power ESD Arc for the temporary sustained event on coupon A during the ESD test at its 15th year age point.

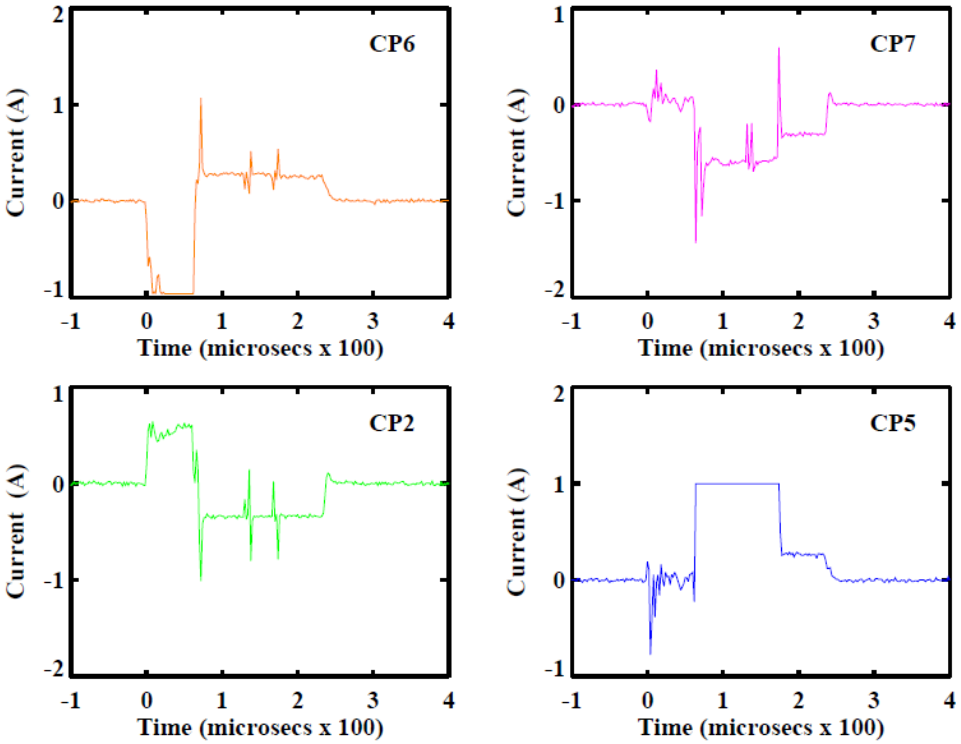

Fig. 20. Measured current for a Full Power ESD Arc for the temporary sustained event on coupon A during the ESD test at its 15th year age point.

C. Thruster Plume Interaction (SPT Interaction) Test Results

Some of the SS/L satellites are equipped with electric propulsion thrusters for station-keeping. The thrusters are typically Hall-Effect Thrusters of the SPT model type (e.g. SPT-100). The SPT thrusters operate by expelling a drifting plasma with 250 eV Xenon ions and low energy (cold) electrons. Using SPT plume models, SS/L determined that the thruster plumes do impinge on the solar array panels. Therefore, SS/L incorporated in their test plan an ion erosion environment (see Fig. 1) and a third type of ESD Arc test called the "SPT Interaction Test". In order to investigate a worst-case ESD scenario, the SPT Interaction Test was scheduled as the last ESD test on coupons that had completed the full 15-year environmental aging cycle. Thus, the thruster plume would interact with the coupons in their most degraded state. A successful SPT Interaction Test, i.e. one without sustained arc generation, would then provide increased margin on the end-of-life performance of the solar array system.

As discussed earlier in Table IV, three different ion flux levels were chosen in order to cover a range of plume impingement scenarios. At each flux level, three "shots" of the Kaufman thruster were executed at each differential string voltage for a total of 18 shots per coupon. Fig. 21 shows a picture of the Kaufman thruster under operation.

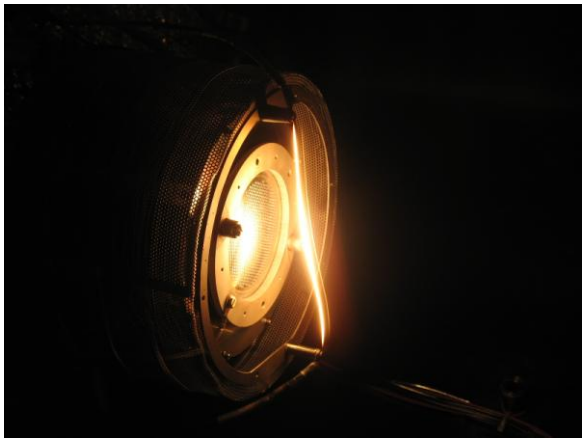

Fig 21. Kaufman thruster under operation.

The SPT Interaction Test procedure extended the procedure used in the Full Power ESD Arc Test. The same conditions for the coupon charging used in the Full Power ESD Arc Test were created in the SPT Interaction test. However, in the SPT interaction test, the electron beam charging process was stopped just before an ESD arc could form. The timing of the electron beam charging was based on the information gathered in the Full Power ESD Arc Test as well as the Arc Inception Voltage Test for a given coupon. With a strong inverted gradient established on the coupon, the thruster plume was applied to the coupon and all of the current probes were monitored for signs of

an ESD arc.

Fig. 22 is a plot of the measured fluxes associated with a typical SPT Interaction Test thruster plume application. The flux measurements are made using a Faraday cup positioned approximately 10 cm below the coupon under test. The plotted data is adjusted to compensate for any spatial variations in the ion flux from the center of the coupon to the actual measurement position. In Fig. 22 one can clearly see the wide dynamic range of fluxes used in the test.

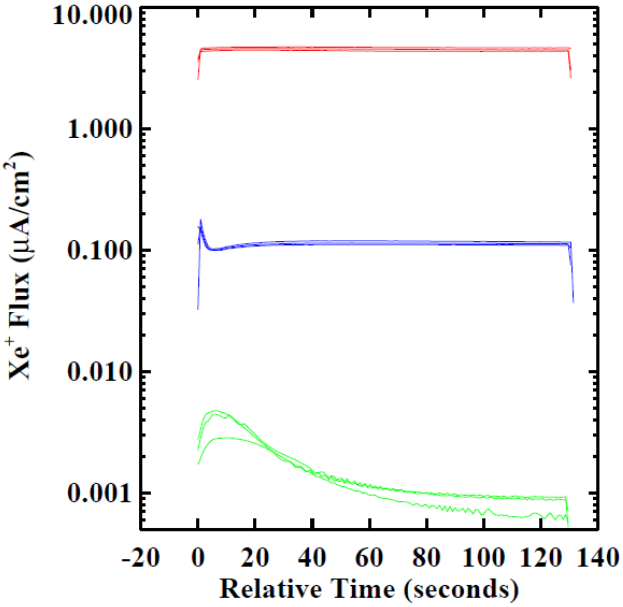

Fig. 22. Composite Faraday Cup data from the SPT interaction test showing all 9 shots for the coupon B 54V string differential condition.

Without exception, an ESD arc was generated on each coupon, at each flux level, as soon as the thruster plume contacted the coupon. The current probe waveforms corresponding to the ESD arc events were no different than those found during the Full Power ESD Arc tests. Also, a scan of the coupon surface potential, after the thruster plume exposure was completed, revealed that the coupon was completely discharged by the thruster plume.

At no time was a sustained or temporary sustained arc detected during the SPT Interaction Test. This is further evidence that the SS/L operational solar array design is not susceptible to sustained arcs even after the equivalent of 15 years of GEO environment exposure.

V. Photovoltaic Cell Performance

A complete evaluation of a space satellite solar array system must include measurements of the photovoltaic cell performance as a function of exposure to the space environment – including the electro-static discharge environment. In this section, data are shown for two diagnostic tests that were used throughout the test campaign to measure any change in the performance of the photovoltaic cells used on the three SS/L test coupons. The diagnostic tests were applied before and after each environmental test exposure.

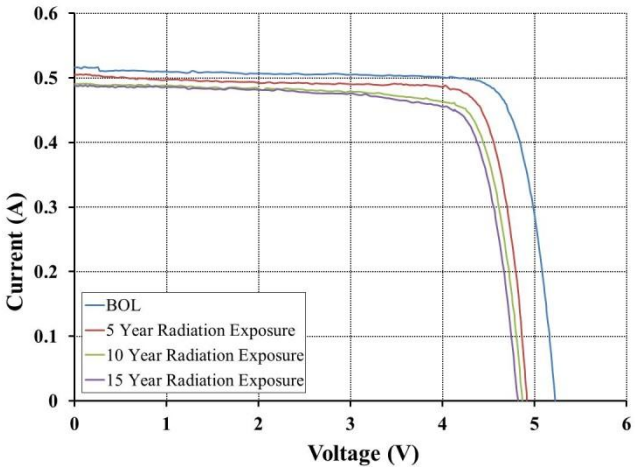

Fig. 23. LAPSS data after each 5-year radiation exposure on coupon A.

The Large Area Pulsed Solar Simulator (LAPSS) diagnostic is designed to measure the power producing capability of photovoltaic cells. A light source, which closely matches the space solar spectrum, illuminates the solar array coupon under test, and the current and voltage generated by the photovoltaic cells is measured. In order to limit the effects of heating on the cell performance, the light is applied in short pulses. Depending on the electrical configuration of the cells on the coupon, the LAPSS data will measure string power production as opposed to individual cell power production. In all of the MSFC tests, two cells were connected in series to form a string. The test coupons contained two strings.

Fig. 23 shows the LAPSS data for one coupon after each 5-year equivalent radiation exposure. The results of the LAPSS tests were in good agreement with the SS/L models for radiation damage.

The only other test to cause a noticeable change in the LAPSS data was the 5th year ion erosion test (see Fig. 24). The cause of the change was due to the removal (erosion) of the anti-reflective coating on the coverglass over each cell. The coating appears to have been completely removed by the first 5-year ion erosion as the 10-year and 15-year data show no change.

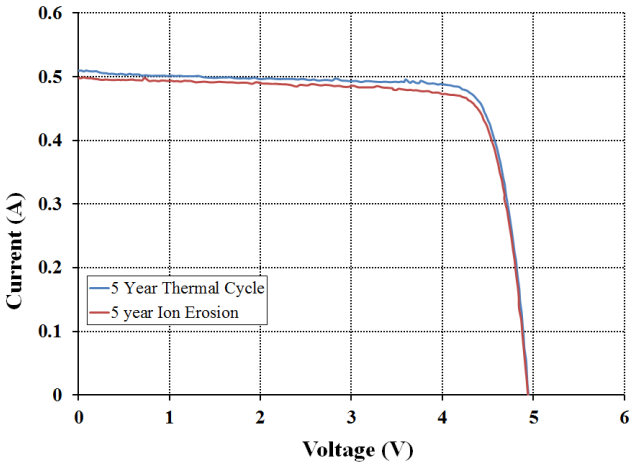

Fig. 24. LAPSS data after each 5-year ion erosion test.

The other diagnostic test used is called "Dark I-V". As the name suggests, the photovoltaic cells are not exposed to light in this test, instead they are in a completely dark environment. Electrical connections are made to the cells/strings and the current "I" is measured as a function of applied voltage "V". The plotted data constitute a characteristic I-V curve. In this type of testing, the cell is treated as an electrical device, e.g. diode or transistor, and changes in its electrical characteristics are in focus, as opposed to its power producing capability.

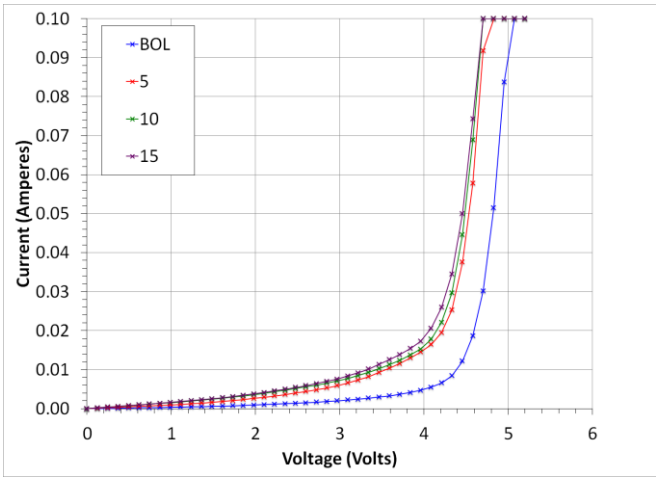

Fig. 25. Dark I-V data after each 5-year radiation exposure on coupon A.

In Fig. 25 the Dark I-V data are shown for one coupon as a function of 5-year equivalent environmental aging. The data show a marked change between the BOL and 5th year increment. However, after the 5th year point, there is little or no significant change.

Although not strictly a photovoltaic component, the bypass diode is often integrated into the cell design. In the case of the SS/L solar arrays, each cell has a bypass diode integrated into the corner of each cell. As such, the bypass diodes are exposed to the same environments as the photovoltaic cells. In a manner similar to the Dark I-V test, the bypass diodes were also tested at regular intervals (after each exposure). Fig. 26 is the test data for one bypass diode as a function of the space environment exposure. In keeping with the trends observed by the LAPPS and Dark I-V tests, the greatest change to the performance of the bypass diode occurred as a result of the first 5-year equivalent environmental exposure.

Overall, the LAPSS and Dark I-V data followed predictable trends. The charged particle radiation tests had the greatest impact on the photovoltaic cell performance as measured by the LAPSS diagnostic. Little or no change in cell performance was noted as a result of Full Power ESD Arc testing. Thus the overall operational design of the SS/L solar array systems appears be well suited to survive the demanding GEO space environment for at least a 15 year lifetime.

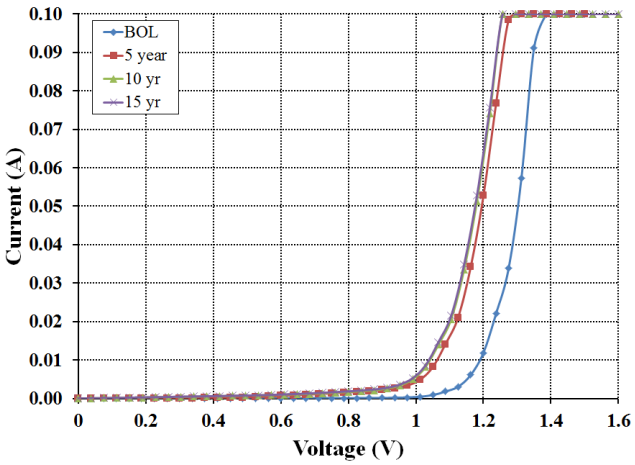

Fig. 26. Bypass diode data after each 5-year radiation exposure on coupon A.

VI. Summary

Space Systems/Loral teamed with NASA's Marshall Space Flight Center to carry out an ambitious test plan which sought to measure the performance of their solar array design throughout the course of 15 years of equivalent space environment exposure. The testing, which required over three calendar years to complete, focused on the performance of three solar array coupons composed of four photovoltaic cells connected to form two independent strings. The coupons were tested and evaluated in 5-year equivalent exposure increments. Each coupon was exposed to ultra-violet radiation, charged particle radiation, thermal cycling, ion erosion, and electro-static discharging environments. After each exposure, diagnostic tests were run to look for any changes in the photovoltaic cell power production. All testing was performed on-site at the Marshall Space Flight Center, which minimized the mechanical stresses on the samples that might have been incurred if multiple shipments to outside laboratories were required.

For the most part, changes in cell performance followed predictable trends and were mostly tied to degradation due to charged particle radiation. The one unexpected result was a dramatic decrease in the Arc Inception Voltage (AIV) after the first 5-year environment exposure. This change has positive implications for GEO solar array systems, as it has the effect of reducing the energy of Electro-static Discharge (ESD) arcs. Based on the consistent lowering of the AIV for all of the test coupons, Space Systems/Loral modified their test plan to recognize the impact of this observation. In the interest of preserving some worst-case test margin, the Space Systems/Loral team did maintain a conservative current level floor for the primary arc pulse applied during Full Power ESD tests.

The ESD arc testing performed throughout the test campaign served a dual role as both an evaluation tool and a space environment. Each coupon was subjected to a minimum of 10 high current ESD arcs per test in order to evaluate the effect of the space environment on charging and discharging characteristics, and to determine if any weak spots existed where arcs tended to concentrate. However, the magnitude of the ESD discharges was sufficiently high that the ESD testing posed a threat to degrade the coupon in a manner similar to the other space environments. Fortunately, no significant changes to the cell performance were documented as a result of the ESD testing. Also, of the approximately 100 ESD arc events generated on each coupon over the length of the test campaign, only one event could be classified as a temporary sustained arc. This suggests that the physical layout of the solar array combined with the nominal operational settings have been optimized to function in the GEO charging environment.

The test campaign results show that the Space Systems/Loral solar array system operational design is robust and able to withstand the GEO environment for at least 15 years. As might be expected, the execution of such a comprehensive engineering test has raised questions about the fundamental factors behind some of the observed changes – particularly in the ESD tests. Answering some of these questions will be the next challenge for the authors and the spacecraft charging test community.

ACKNOWLEDGMENT

The authors would like to thank Dr. D. C. Ferguson of the Air Force Research Laboratory for the discussions during the experimental setup activities. The authors would also like to thank several members of the Space Systems/Loral team including: Bob Neff for his project leadership; Tod Redick for his help with solar array systems operations as well as on-site test support; Ron Corey for his work on ion erosion calculations and SPT interactions; and Roy Tsuji and Mike Staley for their help implementing a high-power solar array simulator supply at MSFC.

REFERENCES

[1] K. Wright, T. Schneider, J. Vaughn, B. Hoang, V.V. Funderburk, F. Wong, G. Gardiner, "Electrostatic Discharge Testing of Multijunction Solar Array Coupons After Combined Space Environmental Exposures" IEEE Trans. Plasma Science, Volume: 40, Issue: 2 , Part: 1, pp. 334 – 344, 2012, DOI: 10.1109/TPS.2011.2174447

[2] M. Stan, D. Aiken, P. Sharps, J. Hills, B. Clevenger, and N. Fatemi, "The Development of >28% Efficient Triple-Junction Space Solar Cells at Emcore Photovoltaics", Paper 3P-B5-03, *3rd World Conference on Photovoltaic Energy Conversion*, Osaka, Japan, May 11-18, 2003.

[3] C. Fetzer, B. Jun, K. Edmondson, S. Khemthong, K. Rouhani, R. Cravens, R. Bardfield, M.Gillanders, "Production ready 30% efficient triple junction space solar cells", *33rd IEEE Photovoltaic Specialists Conference*, 2008, DOI: 10.1109/PVSC.2008.4922620.

[4] X. Zhang, J. Hu, Y. Wu and F. Lu, "Direct observation of defects in triple-junction solar cell by optical deep-level transient spectroscopy" J. Phys. D: Appl. Phys. 42 145401 doi:10.1088/0022-3727/42/14/145401.

[5] A. Bogorad, C. Bowman, P. Papula, S. Mucciacciaro, "Electrostatic discharge induced degradation of solar arrays" *22nd IEEE Photovoltaic Specialists Conference*, 1991, pp. 1531 - 1534 vol.2, DOI: 10.1109/PVSC.1991.169460.

[6] ISO-11221, "Space systems - space solar panels - spacecraft charging induced electrostatic discharge test methods", May 2010.

[7] B. Hoang, F. Wong, V. V. Funderburk, M. Cho, K. Toyoda, and H. Masui, "Electrostatic discharge test with simulated coverglass flashover for multi-junction GaAs/Ge solar array design," *35th IEEE Photovoltaic Specialist Conference*, Honolulu, HI, Jun. 20-25, 2010.

[8] S. Kawakita, M. Imaizumi, M. Takahashi, S. Matsuda, S. Michizono, and Y. Saito, "Influence of high energy electrons and protons on secondary electron emission of cover glasses for space solar cells", Proceeding of *20th International Symposium on Discharges and Electrical Insulation in Vacuum*, Tours, France, July 1-5, 2002, DOI: 10.1109 /ISDEIV.2002.1027315.

[9] R. Corey and D. Pidgeon, "Electric Propulsion at Space Systems/Loral", *31st International Electric Propulsion Conference*, IEPC-2009-270, University of Michigan, Ann Arbor, Michigan, USA, September 20 – 24, 2009.

[10] R. Corey, J. Snyder, X. Price, S. Malone, and T. Randolph, "Hall Thruster Plume Model for Spacecraft Impingement Torque: Development and Validation," J. of Spacecraft and Rockets, vol. 45, no. 4, pps. 766-775, July-Aug. 2008.

[11] H. R. Kaufman and R. S. Robinson, *Operation of Broad-Beam Sources*, Alexandria, Virginia , Commonwealth Scientific Corporation, 1987, pp. 5-8.

[12] H.R. Kaufman, "Technology of Electron-Bombardment Thrusters", in Advances in Electronics and Electron Physics, Vol. 36 (L. Marton, ed.), Academic Press, New York, 1974

[13] E. Amorin, D. Payan, R. Reulet and D. Sarrail, "Electrostatic discharges in a 1m2 solar array coupon – influence of the energy stored on coverglass on flashover current", *9th Spacecraft Charging and Technology Conference*, Tsukuba, Japan, Apr. 4-8, 2005.

[14] H. Masui, T. Endo, K. Toyoda, M. Cho, F. Wong, and B. Hoang, "Electrostatic discharge tests of solar array coupons with different string-to-string gaps without RTV adhesive grout" *11th Spacecraft Charging and Technology Conference*, Albuquerque, NM, Sep. 20-24, 2010.

[15] M. Bodeau, "Current and Voltage Thresholds for Sustained Arcs in Power Systems", IEEE Trans. Plasma Science, Volume: 40 , Issue: 2 , Part: 1, pp. 192-200, 2012, DOI: 10.1109/TPS.2011.2176932XXXX